

発表者氏名	論文タイトル名	発表誌名	巻号	ページ	出版年
Nishimura-Tadaki A, others, <u>Miyake N</u> , Wakui K, Saitu H, Fukushima Y, Hirahara F, <u>Matsumoto N</u> .	Breakpoint determination of X;autosomal balanced translocations in four patients with premature ovarian failure.	J Hum Genet	56(2)	156-160	2011
Tonoki H, others, <u>Matsumoto N</u> , Iizuka S.	Axenfled-Rieger anomaly and Axenfled-Rieger syndrome: clinical, molecular-cytogenetic, and DNA array analyses on three patients with chromosomal defects at 6p25.	Am J Med Genet A	155 (12)	2925-2932	2011
Narumi Y, Shihara T, others, <u>Matsumoto N</u> , Fukushima Y.	Hypomyelination with atrophy of the basal ganglia and cerebellum (H-ABC) in an infant with Down syndrome.	Clin Dysmorphol	20 (3)	166-167	2011
Sakai H, Suzuki S, others, <u>Miyake N</u> , Masuda M, <u>Matsumoto N</u> .	Rapid detection of gene mutations responsible for non-syndromic aortic aneurysm and dissection using two different methods: resequencing microarray technology and next-generation sequencing.	Hum Genet	131(4)	591-599	2011
Saitu H, <u>Matsumoto N</u> .	Genetic commentary: <i>De novo</i> mutations in epilepsies.	Dev Med Child Neurol	53 (9)	806-807	2011

### III. 研究成果の刊行物・別刷

# Mitochondrial Complex III Deficiency Caused by a Homozygous *UQCRC2* Mutation Presenting with Neonatal-Onset Recurrent Metabolic Decompensation

Noriko Miyake,<sup>1\*†</sup> Shoji Yano,<sup>2†</sup> Chika Sakai,<sup>3</sup> Hideyuki Hatakeyama,<sup>3</sup> Yuichi Matsushima,<sup>3</sup> Masaaki Shiina,<sup>4</sup> Yoriko Watanabe,<sup>5</sup> James Bartley,<sup>6</sup> Jose E. Abdenur,<sup>7</sup> Raymond Y. Wang,<sup>7</sup> Richard Chang,<sup>7</sup> Yoshinori Tsurusaki,<sup>1</sup> Hiroshi Doi,<sup>1</sup> Mitsuko Nakashima,<sup>1</sup> Hirotomo Saitsu,<sup>1</sup> Kazuhiro Ogata,<sup>4</sup> Yu-ichi Goto,<sup>3</sup> and Naomichi Matsumoto<sup>1\*</sup>

<sup>1</sup>Department of Human Genetics, Yokohama City University Graduate School of Medicine, Yokohama, Japan; <sup>2</sup>Genetics Division, Department of Pediatrics, LAC+ USC Medical Center, Keck School of Medicine, University of Southern California, Los Angeles, California; <sup>3</sup>Department of Mental Retardation and Birth Defect Research, National Institute of Neuroscience, NCNP, Kodaira, Tokyo, Japan; <sup>4</sup>Department of Biochemistry, Yokohama City University Graduate School of Medicine, Yokohama, Japan; <sup>5</sup>Department of Pediatrics and Child Health, Kurume University School of Medicine, Kurume, Japan; <sup>6</sup>Division of Medical Genetics, Department of Pediatrics, Children's Hospital Los Angeles, Los Angeles, California; <sup>7</sup>Division of Metabolic Disorders, CHOC Children's, Orange, California

Communicated by Daniel Nebert

Received 26 June 2012; accepted revised manuscript 7 November 2012.

Published online 19 December 2012 in Wiley Online Library (www.wiley.com/humanmutation). DOI: 10.1002/humu.22257

**ABSTRACT:** Mitochondrial complex III (CIII) deficiency is a relatively rare disease with high clinical and genetic heterogeneity. CIII comprises 11 subunits encoded by one mitochondrial and 10 nuclear genes. Abnormalities of the nuclear genes such as *BCS1L* and *TTC19* encoding mitochondrial assembly factors are well known, but an explanation of the majority of CIII deficiency remains elusive. Here, we report three patients from a consanguineous Mexican family presenting with neonatal onset of hypoglycemia, lactic acidosis, ketosis, and hyperammonemia. We found a homozygous missense mutation in *UQCRC2* that encodes mitochondrial ubiquinol-cytochrome *c* reductase core protein II by whole-exome sequencing combined with linkage analysis. On the basis of structural modeling, the mutation (p.Arg183Trp) was predicted to destabilize the hydrophobic core at the subunit interface of the core protein II homodimer. In vitro studies using fibroblasts from the index patient clearly indicated CIII deficiency, as well as impaired assembly of the supercomplex formed from complexes I, III, and IV. This is the

first described human disease caused by a core protein abnormality in mitochondrial CIII.

Hum Mutat 00:1–10, 2012. © 2012 Wiley Periodicals, Inc.

**KEY WORDS:** mitochondrial complex III (CIII); *UQCRC2*; whole exome sequence; supercomplex

## Introduction

The mitochondrial respiratory chain generates energy as ATP by means of the electron-transport chain and the oxidative-phosphorylation system. The mitochondrial respiratory chain, located in the inner mitochondrial membrane, is composed of five multimeric protein complexes: I, II, III, IV, and V. Among them, the complex III (CIII) (bc<sub>1</sub> complex or ubiquinol-cytochrome *c* reductase; EC1.10.2.2) monomer is composed of 11 proteins [Iwata et al., 1998]. One protein is encoded by mitochondrial DNA (*MTCYB*) and the other 10 are encoded by nuclear DNA. The latter are categorized into three groups: (1) core proteins (encoded by *UQCRC1* and *UQCRC2*), (2) respiratory proteins (*CY1* and *UQCRFS1*), and (3) low-molecular-weight proteins (*UQCRH*, *UQCRB*, *UQCRQ*, *UCRC*, *UQCR11*, and *UQCRFS1*). In its native state, the CIII monomer is quickly converted into a catalytically active homodimer that is incorporated into a supercomplex (respirasome) with complexes I and IV, and this supercomplex functions as a single enzyme [Schagger and Pfeiffer, 2000].

Mitochondrial CIII enzyme deficiency (CIII deficiency; MIM# 124000) is a relatively rare disease with clinical and genetic heterogeneity. Until now, mutations in four genes have been known to cause autosomal recessive CIII deficiencies: *UQCRB* (NM\_006294), *UQCRQ* (NM\_014402), *BCS1L* (NM\_004328), and *TTC19* (NM\_017775). *UQCRB* and *UQCRQ* encode components of CIII itself, whereas *BCS1L* and *TTC19* produce mitochondrial assembly factors. Although recessive *BCS1L* mutations are the most frequent cause of CIII deficiency, the majority of the genetic causes of CIII deficiency remain unknown [Benit et al., 2009; de Lonlay et al.,

Additional Supporting Information may be found in the online version of this article.

<sup>†</sup>These authors contributed equally to this work.

\*Correspondence to: Noriko Miyake, Department of Human Genetics, Yokohama City University Graduate School of Medicine, 3-9 Fukuura, Kanazawa-ku, Yokohama 236-0004, Japan. E-mail: Noriko Miyake: nmiyake@yokohama-cu.ac.jp; or Naomichi Matsumoto, Department of Human Genetics, Yokohama City University Graduate School of Medicine, 3-9 Fukuura, Kanazawa-ku, Yokohama 236-0004, Japan. E-mail: naomat@yokohama-cu.ac.jp

Contract grant sponsors: Ministry of Health, Labor, and Welfare; the Japan Science and Technology Agency; the Strategic Research Program for Brain Sciences; Ministry of Education, Culture, Sports, Science, and Technology of Japan; the Japan Society for the Promotion of Science; 2011 Strategic Research Promotion of Yokohama City University; the Japan Epilepsy Research Foundation; and the Takeda Science Foundation.

2001; DiMauro and Schon, 2003; Fernandez-Vizarrá et al., 2007; Hinson et al., 2007; Visapaa et al., 2002]. Interestingly, *BCS1L* mutations cause variable clinical presentations: Bjornstad syndrome (MIM# 262000), which is characterized by sensorineural hearing loss and pili torti [Hinson et al., 2007]; GRACILE syndrome (MIM# 603358), which presents with fetal growth retardation, aminoaciduria, cholestasis, iron overload, lactic acidosis, and early death [Visapaa et al., 2002]; and Leigh syndrome (MIM# 256000) [de Lonlay et al., 2001]. A homozygous mutation of *TTC19* causes a progressive neurodegenerative disorder [Ghezzi et al., 2011]. A homozygous 4-bp deletion of *UQCRB* causes hypoglycemia and lactic acidosis [Haut et al., 2003] and a homozygous missense mutation of *UQCRQ* results in severe psychomotor retardation, extrapyramidal signs, and dementia [Barel et al., 2008].

Here, we describe the first human mutation of *UQCRC2* encoding core protein 2 of CIII, utilizing linkage analysis and whole-exome sequencing.

## Materials and Methods

### DNA Preparation

DNAs from family members and fibroblasts from patients were collected after obtaining informed consent. DNA was extracted from blood leukocytes using a QIAamp DNA Blood Midi Kit (Qiagen, Hilden, Germany) or QuickGene-610L (Fujifilm, Tokyo, Japan), according to the manufacturers' instructions. DNAs from 80 Mexican control subjects were purchased from the Coriell Institute for Medical Research (Camden, New Jersey). The experimental protocols were approved by the institutional review board of Yokohama City University.

### Linkage Analysis

SNP typing was performed using an Affymetrix Human Mapping SNP 10K Xba I 142 2.0 array (Affymetrix, Santa Clara, California), according to the manufacturer's instructions. A multipoint linkage analysis was performed using Allegro version 2.0 [Gudbjartsson et al., 2005]. An autosomal recessive mode of inheritance with complete penetrance and a disease allele frequency of 0.005 was used.

### Exome Sequence

Briefly, 3  $\mu$ g of genomic DNA was sheared and captured using a NimbleGen SeqCap EZ Exome Library SR (Roche NimbleGen, Inc., Madison, New Jersey), according to the manufacturer's instructions. The captured sample was sequenced on a GAIx instrument (Illumina, Inc., San Diego, California) using 76-bp paired-end reads. Image analysis and base calling were performed by sequence-control software real-time analysis (Illumina, Inc.) and CASAVA software v1.7 (Illumina, Inc.). The quality-controlled (path-filtered) reads were mapped to human genome reference hg19 with Mapping and Assembly with Qualities (MAQ; <http://maq.sourceforge.net/>) and NextGENe software v2.00 (SoftGenetics, State College, Pennsylvania). The variants from MAQ were annotated by SeattleSeq annotation 131 (<http://snp.gs.washington.edu/SeattleSeqAnnotation131>). The priority scheme of the variants was described previously [Tsurusaki et al., 2011]. The nucleotide numbering of the variants reflects the cDNA numbering, with +1 corresponding to the A of the ATG translation initiation codon in the reference sequence, accord-

ing to journal guidelines ([www.hgvs.org/mutnomen](http://www.hgvs.org/mutnomen)). The initiation codon is codon 1.

### Expression Vector Preparation

For construction of a mammalian expression vector, full-length *UQCRC2* (NM\_003366.2) was amplified from a cDNA library from a multiple-tissue cDNA (MTC) panel (Clontech, Mountain View, California) using KOD-plus DNA polymerase (Toyobo, Osaka, Japan). The PCR product was cloned into the entry vector (pDONR<sup>TM</sup>221) of the gateway system (Invitrogen, Carlsbad, California). Each of the two missense mutations was independently introduced into the entry clone using a QuickChange II XL site-directed mutagenesis kit (Stratagene, La Jolla, California). Each insert was cloned into pcDNA-DEST40 (C-terminal V5 and 6xHis tag) by LR recombination. All the clones were verified by direct sequencing. In addition, full-length *UQCRC2* (wild type, mutant, or SNP [rs4850: c.548G>A, p.Arg183Gln]) and AcGFP constructs were cloned into multiple cloning sites A and B of the pIRES vector (Clontech).

### Intracellular Localization

Each mammalian expression construct (200 ng) was transfected into COS-1 cells using FuGENE6 (Roche Diagnostics, Indianapolis, Indiana). After 24 hr of transfection, MitoTracker Red CMXRos (Invitrogen) was added and incubated for 30 min. The cells were then fixed with 4% paraformaldehyde for 20 min at room temperature. After permeabilization with 0.1% Triton/1 $\times$  PBS for 10 min, C-terminally V5-6xHis-tagged *UQCRC2* protein was stained with a mouse anti-V5 antibody (1:1,000) (Invitrogen) and an Alexa Fluor 488-conjugated goat antimouse IgG secondary antibody (1:1,000) (Molecular Probes, Carlsbad, California). Confocal images were taken with a FLUOVIEW FV1000-D microscope (Olympus, Tokyo, Japan).

### Mitochondrial Enzyme Activity Assay

Mitochondrial enzyme activities were measured using a previously reported method [Trounce et al., 1996], with slight modifications. The complex I activity is indicated as the rotenone-sensitive NADH-CoQ1 reductase activity. In control assays, the activity was decreased to 20% by rotenone.

### Western Blotting

Mitochondrial enzyme activity and supercomplex formation were analyzed by western blotting. The enzyme activities of the mitochondrial respiratory chain complexes were measured using mitochondrial fractions prepared from primary fibroblasts derived from patient 1 ( $n = 3$ ) and control subjects ( $n = 10$ ). Each measurement was basically performed in triplicate (if the available materials allowed). The values were normalized to complex II or citrate synthase. Immunoblot detection of each respiratory chain complex was performed using mitochondria solubilized with 0.5% *n*-dodecyl- $\beta$ -D-maltoside (DDM). The same amount of pooled mitochondrial protein from control subjects ( $n = 10$ ) was used as the control. The primary antibodies used were as follows: 2  $\mu$ g/ml anti-NDUFA9 (complex I; Invitrogen), 0.02  $\mu$ g/ml anti-SDHA (complex II; Invitrogen), 2  $\mu$ g/ml anti-UQCRC1 (CIII; Abcam, Cambridge, Massachusetts), 0.2  $\mu$ g/ml anti-MTCO1 (complex IV; Invitrogen), and

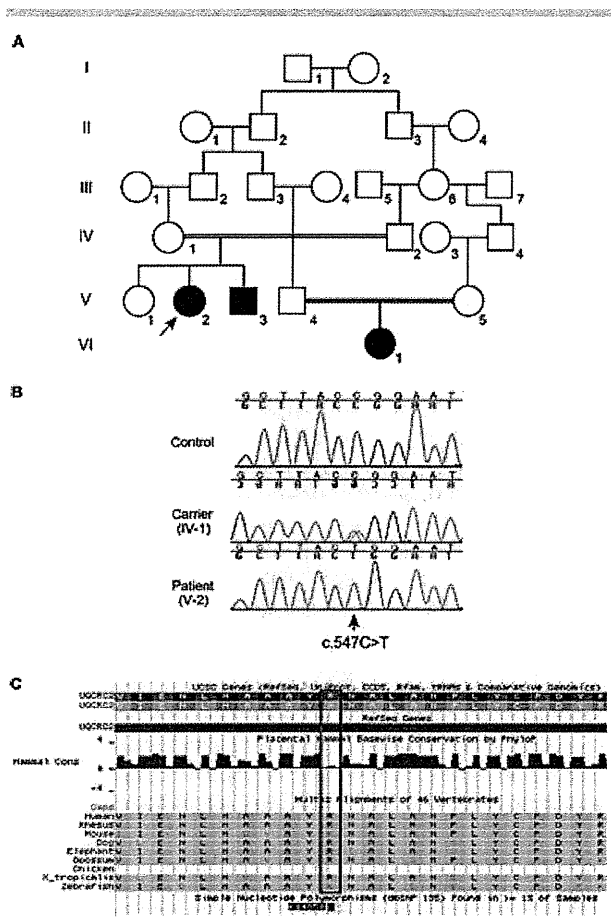


**Figure 1.** Identification of a *UQCRC2* mutation in a consanguineous Mexican family. **A:** Pedigree of the reported family. The arrow indicates the proband. **B:** Electropherogram of the c.547C>T *UQCRC2* mutation. All three patients (1, 2, and 3) showed a homozygous change, whereas the parents and an unaffected sibling of patients 1 and 2 were heterozygous carriers. The arrow indicates c.547C>T. **C:** Evolutionary conservation of p.Arg183 in *UQCRC2* outlined in red. rs4850 (chr 16: 21976762, G>A, p.Arg183Gln) is a common SNP based on the dbSNP135 database.

2 µg/ml anti-ATP5B (complex V; Invitrogen). Immunoblot detection of the respiratory supercomplex was performed using mitochondria solubilized with 1% (w/v) digitonin. The same amount of pooled mitochondrial protein from control subjects (*n* = 10) was used as the control. The primary antibodies used were as follows: 0.02 µg/ml anti-SDHA (complex II; Invitrogen) and 2 µg/ml anti-UQCRC1 (CIII; Abcam). The band intensity of the supercomplex was estimated by densitometry and normalized to that of complex II. The data were obtained by three independent assays.

**Results**

Patient 1 (V:2 in Fig. 1A) is a Hispanic female born to a 26-year-old healthy female (G2P2Ab0) and a 28-year-old healthy male who are second cousins. She was delivered at 37 weeks by Cesarean section because of a pathological cardiotocogram. At birth, she weighed 2,329 g (5–10th percentile) with a length of 46 cm (5–10th percentile), and her occipitofrontal circumference was 34 cm (25–50th percentile). Her Apgar scores were 8, 9, and 9 at 1, 5, and 10 min, respectively. She developed a severe metabolic acidosis

(pH 7.1, with a base excess of –24.6 mEq/l) within 1 day, requiring admission to a neonatal intensive care unit. Blood lactate and pyruvate on admission were 25.5 mM (reference range: <2.2 mM) and 0.436 mM (reference range: <0.16 mM), respectively (lactate to pyruvate ratio = 58.48). Clinical examination revealed tachypnea (47 breaths/min), tachycardia (181 beats/min), mild subcostal retractions, Levine II/VI systolic cardiac murmur, no organomegaly, and poor sucking reflex. Blood ammonia was 126 µM (reference range in neonates: <80 µM). The patient responded promptly to supportive therapy, with intravenous glucose infusion providing 10 mg/kg/min and a sodium bicarbonate drip improving the blood lactate level down to 12.7 mM within 24 hr. The lactate and pyruvate levels further improved to 3.1 and 0.125 mM within 3 days, respectively. Urine organic acid analysis on admission was remarkable for massive lactic and pyruvic aciduria, as well as ketonuria. Plasma amino acids were remarkable for a high alanine level (1,519 µM; reference range: 200–600 µM). Magnetic resonance imaging (MRI) of the brain revealed small right parietal and temporal infarcts.

She recovered without sequelae and was discharged on full oral feeds with a high-carbohydrate, reduced-fat formula (60% of calories from carbohydrate, 30% of calories from fat) after 1.5 months of hospitalization. She was also diagnosed with an atrial septal defect and renal tubular acidosis. After the initial hospitalization, she was hospitalized more than 10 times because of episodic metabolic decompensation with lactic acidosis (highest value was 10.8 mM at the age of 3 years and 10 months), hyperammonemia (highest value was 346 µM at the age of 3 years and 3 months), ketosis, and hypoglycemia, which were triggered by intercurrent illnesses including fevers, vomiting, and diarrhea. The patient is now 5 years of age, with normal growth and no signs of intellectual disability. The frequency of hospitalization has decreased, although she still requires urgent medical treatment with intravenous glucose infusion to prevent metabolic decompensation during intercurrent illnesses.

Patient 2 (V:3 in Fig. 1A) is a younger full sibling of patient 1. He was born at 39 weeks of gestation by repeat Cesarean section. At birth, he weighed 2,658 g (5–10th percentile) with a length of 49 cm (25–50th percentile), and his occipitofrontal circumference was 34.3 cm (25th percentile). His Apgar scores were 8 and 9 at 1 and 5 min, respectively. He developed tachypnea, grunting, and poor feeding within 1 day because of lactic acidemia. The initial capillary blood gas showed a pH of 7.05, pCO<sub>2</sub> of 25 mmHg, bicarbonate of 5.8 mmol/l, and a base excess of –22 mEq/l. He was intubated for 2 days and treated with intravenous glucose infusion and a bicarbonate drip to correct the metabolic acidosis. Feeding with a high-carbohydrate, reduced-fat formula was started in 10 days. His initial hospitalization was 1-month long, during which he was diagnosed with congenital lactic acidemia and persistent hypoglycemia of unknown etiology. He was treated with corticosteroid replacement therapy owing to adrenal insufficiency for 4 months until a normal adrenocorticotropic hormone stimulation test was obtained. At the age of 8 months, he was found unresponsive after 6 hr of fasting owing to decreased appetite associated with a 2-day mild upper-respiratory-tract infection. At a local emergency room, metabolic acidosis (pH 7.23), hypoglycemia (3 mg/dl; reference range: >60 mg/dl), and hyperammonemia (463 µM), as well as ketosis (blood and urine), were noted. He had five episodes of generalized seizure associated with this episode. Following treatment with levetiracetam, he has been seizure free. Brain MRI findings at the age of 8 months were unremarkable. He was hospitalized for 1 month and discharged without sequelae, and had more than 10 hospitalizations because of similar episodes of lactic acidosis, hypoglycemia, hyperammonemia, and ketosis triggered by intercurrent illnesses. Developmental delay was noted once at 4 months of age. Following

physical and speech therapy, his development was later evaluated as normal at 3 years of age. He is now 4 years of age, with normal growth and no signs of intellectual disability. Physical examination revealed neither dysmorphic features nor abnormal focal neurological signs. He has been fed with a reduced-fat, high-carbohydrate diet and fasting precautions. The frequency of hospitalization has decreased, although he continues to require urgent medical treatment with intravenous glucose infusion to prevent metabolic decompensation during intercurrent illnesses. Laboratory study data obtained in the acute severe metabolic decompensation stage at 16 months of age were remarkable, which are as follows: pH 7.19 capillary blood gas, 11 mg/dl glucose, 348  $\mu$ M blood ammonia, and 6.8 mM blood lactate. Urine organic acid analysis showed markedly elevated 3-hydroxybutyrate and acetoacetate indicating severe ketosis, markedly elevated lactate and pyruvate indicating lactic acidosis, markedly elevated dicarboxylic acids (adipic acid, 1,194 mmol/mol Cr [reference range: <15 mmol/mol Cr], suberic acid, 122 mmol/mol Cr [reference range: <7 mmol/mol Cr], sebacic acid, 288 mmol/mol Cr [reference range: <2 mmol/mol Cr]) indicating hyperactive fatty acid beta oxidation, and moderately elevated tricarboxylic acid cycle intermediates including malate, fumarate, and 2-oxoglutarate. Plasma amino acids showed elevated alanine at 440  $\mu$ M (reference range: 23–410  $\mu$ M). Acylcarnitine profiles obtained at 19 months of age in mild decompensation showed marked elevation of C2 (48 nmol/ml [reference range: 2.6–15.5 nmol/ml]) and moderate elevation of 3-hydroxyacylcarnitines (C12–C18).

Patient 3 (VI:1 in Fig. 1A) is a girl born to consanguineous parents within the same pedigree as patients 1 and 2, but in a different branch. She was small for gestational age and was born vaginally to a 23-year-old mother after a full-term gestation. Her birth weight was 2,200 g. Initially, she had mild respiratory distress and required 1 additional day of monitoring. By 18 months of age, she had undergone four hospitalizations for vomiting, dehydration, and hypoglycemia. An initial blood examination at 18 months of age showed that her blood glucose was 17 mg/dl, bicarbonate was 8 mmol/l, and anion gap was 30 mmol/l. The simultaneous blood lactate and pyruvate levels were 26.3 mg/dl (reference range: <16.0 mg/dl) and 1.5 mg/dl (reference range: <1.5 mg/dl), respectively. She responded quickly to intravenous dextrose with correction of the hypoglycemia and metabolic acidosis. She had developmental delay and microcephaly (second percentile) that led to a brain MRI, but this was interpreted as normal. At 18 months, she spoke only two words but could follow two-part commands. She walked at 15 months of age and had low body weight until starting occupational therapy at 14 months of age. She was not dysmorphic. Her muscle strength and tone were normal when she was in good health, allowing her to climb, hop, and jump in a manner appropriate for her age.

Considering the consanguinity in this family, we hypothesized that the disease was inherited in an autosomal recessive fashion. Linkage analysis using two patients (1 and 2) and three unaffected family members (IV:1, IV:2, and V:1) indicated that homozygous regions totaling 36-Mb were shared by the two affected individuals with logarithm of the odds scores  $\geq 2.0$ , as calculated by Allegro version 2 [Gudbjartsson et al., 2005] (Supp. Table S1). We then performed whole-exome sequencing of DNA from patient 1. Two homozygous variants within the 36-Mb homozygous regions were identified: c.547C>T, p.Arg183Trp in *UQCRC2* (NM\_003366) and c.1675A>G, p.Met559Val in *TNRC6A* (NM\_014494). Sanger sequencing confirmed the two variants in patient 1. The Polyphen-2 program (<http://genetics.bwh.harvard.edu/pph2/>) predicted that p.Arg183Trp in *UQCRC2* and p.Met559Val in *TNRC6A* were probably damaging and benign, respectively (Table 1). *TNRC6A* was

**Table 1. Prediction of Mutational Effects in UQCRC2**

Mutation	Alteration	Type	Grantham score <sup>a</sup>	Polyphen-2	Energy ddG <sup>b</sup>
c.547C>T	p.Arg183Trp	Mutant	101	0.998	10.02
c.548G>A	p.Arg183Gln	SNP	43	0.177	2.19
c.547_548CG>AA	p.Arg183Lys	Ortholog	26	0.001	1.74

<sup>a</sup>Grantham score indicates the chemical dissimilarity caused by codon replacements.  
<sup>b</sup>The corrected average interaction energy ddG of each altered amino acid is calculated by FoldX as homozygous mutation.

ruled out as a candidate because the heterozygous *TNRC6A* change was found in patient 3. *UQCRC2* encodes ubiquinol-cytochrome *c* reductase core protein II (*UQCRC2*; MIM# 191329), a core protein of CIII. All three patients possessed the homozygous p.Arg183Trp change in *UQCRC2*, whereas the father (IV-2), mother (IV-1), and sister (V-1) (all unaffected) were heterozygous (Fig. 1B). This change was not observed among 80 Mexican control alleles or 750 Japanese control alleles.

To predict the effect of the missense mutation (c.547C>T, p.Arg183Trp) on the structural stability of CIII, we calculated the free-energy change of interactions between the core protein monomers (encoded by *UQCRC2*) with and without the mutation using FoldX software (version 3.0) [Guerois et al., 2002; Khan and Vihinen, 2010]. For this calculation, we used the crystal structure of bovine CIII (PDB code 2A06) as a structural model because no crystal structure is available for human *UQCRC2*. Amino acid position 183 of *UQCRC2* is a highly conserved basic amino acid among species from zebrafish to humans (e.g., Arg in humans and cows, Lys in mice; Fig. 1C) and is reported to be substituted for Gln as a nonsynonymous human SNP (rs4850 [c.548G>A, p.Arg183Gln]) (Fig. 1C). Therefore, we also calculated the interaction-energy change upon replacement of Arg183 with Lys or Gln, in addition to the Trp found in the patient. The calculated interaction-energy change caused by replacement of Arg183 with Trp was estimated as 10 kcal/mol, whereas those caused by replacement with Lys or Gln were no more than 2 kcal/mol (Fig. 2A, Table 1). The molecular structure of the wild-type core protein homodimer indicated that the methylene part of the Arg183 side chain of one subunit forms a hydrophobic core with the side chains of His254 and Phe449 of the other subunit at the homodimer interface (Fig. 2B and C). When the Arg183 of the core protein was replaced by Trp, the introduced Trp183 side chain flipped outward from the original side-chain position because of steric hindrance (Fig. 2D). In contrast, when Arg183 was replaced by Lys or Gln, each side chain occupied the original position to maintain a hydrophobic core with the methylene part of Lys or Gln (Fig. 2E and F). This indicates that the Arg183Trp mutation in *UQCRC2* would disrupt the hydrophobic core formed at the interface of the *UQCRC2*-containing complex, resulting in destabilization of CIII. In vitro experiments showing that the exogenous and endogenous expressions of the *UQCRC2* mutant were significantly reduced (Supp. Figs. S1 and S2) may support the protein instability.

To test whether this mutation alters *UQCRC2* localization at the mitochondrial inner membrane, we created mammalian full-length wild-type, mutant, and SNP (rs4850) constructs; transiently overexpressed them in COS1 cells; and observed their localization microscopically. The mutant protein colocalized with mitochondria, similar to the wild-type and SNP proteins (Supp. Fig. S3). This indicates that the p.Arg183Trp mutation probably does not alter the intracellular localization.

To evaluate mitochondrial function in vitro, we measured the enzyme activities of the mitochondrial respiratory chain complexes

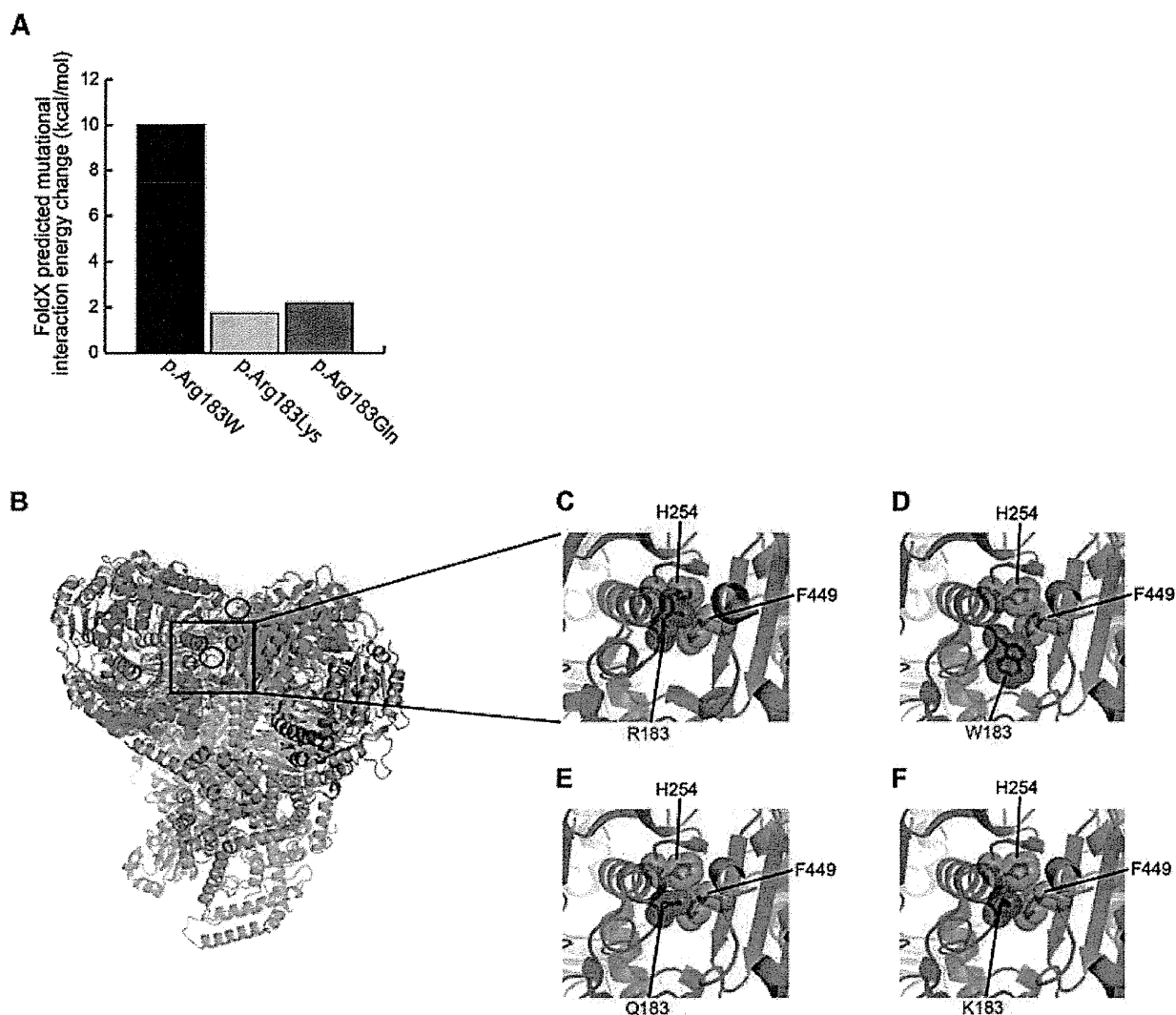


**Figure 2.** Molecular structural consideration of the effect on dimerization of amino acid replacement at residue position 183 in the core protein. **A:** Calculated interaction-energy change of the core protein homodimer upon replacement by the indicated amino acids at residue 183 using FoldX software. **B:** Overview of the crystal structure of the bovine mitochondrial bc1 (CIII) complex (PDB code 2A06). The core protein monomers are colored green and cyan; the other components are shown in gray. The helices, strands, and loops are shown as ribbons, arrows, and threads, respectively. The red circle indicates residue 183 in the core protein. The box corresponds to the enlarged areas shown in parts (C)–(F). **C–F:** Detailed views of the core protein homodimerization interface in the wild-type (C) and mutated, polymorphic, orthologous (p.Arg183Trp/Gln/Lys) (D, E, F, respectively) complex structures. The residues at amino acid 183 of one subunit (red), and His254 and Phe449 of the other subunit (orange) are shown as sticks with Connolly surfaces. All graphics were drawn using PyMOL ([www.pymol.com](http://www.pymol.com)).

using mitochondrial fractions prepared from primary fibroblasts derived from patient 1. With normalization to complex II activity, the CIII activity of patient 1 was decreased to 50% of that in the control subjects ( $n = 10$ ), whereas complex I activity increased by threefold and complex IV activity remained at the same level as in the control subjects (Fig. 3A). Similar results were obtained using normalization to citrate synthase activity (Fig. 3B). We also investigated the steady-state level of the respiratory complexes by blue-native polyacrylamide gel electrophoresis (BN-PAGE) using the same mitochondrial fraction used for the enzyme activity measurements. For analysis of individual complexes, mitochondria were solubilized with 0.5% (w/v) DDM. For analysis of the supercomplex (complexes I, III, and IV), mitochondria were solubilized with 1% (w/v) digitonin. After BN-PAGE, we performed immunoblotting with specific antibodies for the respi-

ratory complexes (Fig. 3C–F, Supp. Notes, and Supp. Fig. S4). In the patient's fibroblasts, we found that CIII and supercomplex assembly were decreased to 18%–20%  $\gg$  22%–23% (Fig. 3C and D) and 4%  $\gg$  7.5% (Fig. 3E and F) of the levels in pooled control samples, respectively. These data indicate that a homozygous missense mutation (c.547C>T, p.Arg183Trp) in *UQCRC2* causes moderately impaired CIII function and severely decreased amounts of CIII and supercomplex, which would be the primary molecular pathogenesis in the patients.

## Discussion

Among the genes known to cause CIII deficiency, impairment of *UQCRC2*, as found in our patients, leads to a similar clinical course to that reported for *UQCRB* defects with recurrent crises of

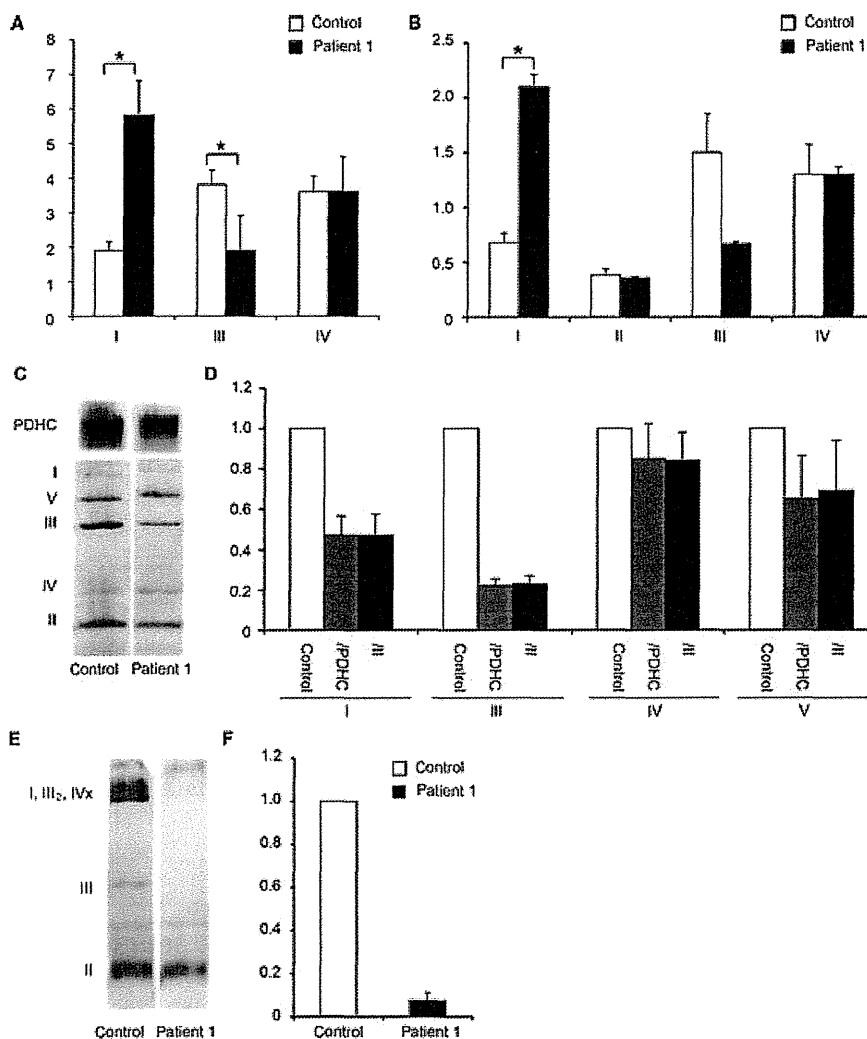


**Figure 3.** Mitochondrial enzyme activity and supercomplex formation. **A, B:** Enzyme activities of the mitochondrial respiratory chain complexes using mitochondrial fractions prepared from primary fibroblasts derived from patient 1 ( $n = 3$ ) and control subjects ( $n = 10$ ). Each measurement was performed in triplicate. The values were normalized to complex II (**A**) or citrate synthase (**B**). Error bars represent the SEM. **C, D:** Immunoblot detection of each respiratory chain complex using mitochondria solubilized with 0.5% DDM. The same amount of pooled mitochondrial protein from control subjects ( $n = 10$ ) was loaded into the control lane. The band intensity of each respiratory complex was estimated by densitometry and normalized to that of PDHC (gray bar) or complex II (black bar). The data were obtained by three independent assays and the error bars in (**D**) represent the SEM. **E, F:** Immunoblot detection of the respiratory supercomplex using mitochondria solubilized with 1% (w/v) digitonin. The same amount of pooled mitochondrial protein from control subjects ( $n = 10$ ) was loaded into the control lane. The band intensity of the supercomplex was estimated by densitometry and normalized to that of complex II (black bar). The data were obtained by three independent assays and the error bars in (**F**) represent the SEM.

hypoglycemia, lactic acidosis, and ketosis, although the latter did not show hyperammonemia. In contrast, impairment of BCS1L, TTC19, and UQCRC2 leads to rather severe complications such as intrauterine growth retardation, liver failure, tubulopathy, sensorineural hearing loss, and abnormalities on brain MRI. The normal development in our patients, despite frequent metabolic crises, may suggest that the UQCRC2 phenotype in our family is milder than disorders of the CIII genes and that this UQCRC2 abnormality does not primarily affect the brain. However, patients 2 and 3 showed epilepsy, and developmental delay was noted in patient 3. It remains to be seen whether this clinical variability is caused by variable expressivity, unknown modifiers, or secondary to the severity of the acute metabolic crises. Interestingly, our patients showed hyperammonemia, highly abnormal urine organic acids indicative

of mitochondrial dysfunction, and highly elevated plasma hydroxyl fatty acids during their crises, whereas patients with the other reported CIII impairment disorders did not [Barel et al., 2008; de Lonlay et al., 2001; Ghezzi et al., 2011; Haut et al., 2003; Hinson et al., 2007; Visapaa et al., 2002]. These observations may imply that UQCRC2 mutations have secondary effects in other metabolic pathways including the Krebs cycle, beta oxidation, and urea cycle.

## Conclusion

We have identified, for the first time, a homozygous mutation in human UQCRC2 encoding a core protein of mitochondrial CIII. Further studies of additional patients with UQCRC2 abnormalities are necessary to fully understand human CIII disorders.



## Acknowledgments

We thank all the family members for participating in this study. We also thank the Commission for Families and Children of Orange County for its support of our clinical work. We appreciate Dr. Takeyori Saheki for useful comments on metabolic decompensation. This study was performed at the Advanced Medical Research Center, Yokohama City University.

*Disclosure statement:* The authors have no conflict of interest to declare.

## References

- Barel O, Shorer Z, Flusser H, Ofir R, Narkis G, Finer G, Shalev H, Nasara A, Saada A, Birk OS. 2008. Mitochondrial complex III deficiency associated with a homozygous mutation in UQCRCQ. *Am J Hum Genet* 82:1211–1216.
- Benit P, Lebon S, Rustin P. 2009. Respiratory-chain diseases related to complex III deficiency. *Biochim Biophys Acta* 1793:181–185.
- de Lonlay P, Valnot I, Barrientos A, Gorbatyuk M, Tzagoloff A, Taanman JW, Benayoun E, Chretien D, Kadhom N, Lombes A, de Baulny HO, Niaudet P, et al. 2001. A mutant mitochondrial respiratory chain assembly protein causes complex III deficiency in patients with tubulopathy, encephalopathy and liver failure. *Nat Genet* 29:57–60.
- DiMauro S, Schon EA. 2003. Mitochondrial respiratory-chain diseases. *N Engl J Med* 348:2656–2668.
- Fernandez-Vizarra E, Bugiani M, Goffrini P, Carrara F, Farina L, Procopio E, Donati A, Uziel G, Ferrero I, Zeviani M. 2007. Impaired complex III assembly associated with BCS1L gene mutations in isolated mitochondrial encephalopathy. *Hum Mol Genet* 16:1241–1252.
- Ghezzi D, Arzuffi P, Zordan M, Da Re C, Lamperti C, Benna C, D'Adamo P, Diodato D, Costa R, Mariotti C, Uziel G, Smiderle C, et al. 2011. Mutations in TTC19 cause mitochondrial complex III deficiency and neurological impairment in humans and flies. *Nat Genet* 43:259–263.
- Gudbjartsson DF, Thorvaldsson T, Kong A, Gunnarsson G, Ingólfssdóttir A. 2005. Allegro version 2. *Nat Genet* 37:1015–1016.
- Guerois R, Nielsen JE, Serrano L. 2002. Predicting changes in the stability of proteins and protein complexes: a study of more than 1000 mutations. *J Mol Biol* 320:369–387.
- Haut S, Brivet M, Touati G, Rustin P, Lebon S, Garcia-Cazorla A, Saudubray JM, Boutron A, Legrand A, Slama A. 2003. A deletion in the human QP-C gene causes a complex III deficiency resulting in hypoglycaemia and lactic acidosis. *Hum Genet* 113:118–122.
- Hinson JT, Fantin VR, Schonberger J, Breivik N, Siem G, McDonough B, Sharma P, Keogh I, Godinho R, Santos F, Esparza A, Nicolau Y, et al. 2007. Missense mutations in the BCS1L gene as a cause of the Bjornstad syndrome. *N Engl J Med* 356:809–819.
- Iwata S, Lee JW, Okada K, Lee JK, Iwata M, Rasmussen B, Link TA, Ramaswamy S, Jap BK. 1998. Complete structure of the 11-subunit bovine mitochondrial cytochrome bc1 complex. *Science* 281:64–71.
- Khan S, Vihinen M. 2010. Performance of protein stability predictors. *Hum Mutat* 31:675–684.
- Mitsuhashi S, Hatakeyama H, Karahashi M, Koumura T, Nonaka I, Hayashi YK, Noguchi S, Sher RB, Nakagawa Y, Manfredi G, Goto Y, Cox GA, Nishino I. 2011. Muscle choline kinase beta defect causes mitochondrial dysfunction and increased mitophagy. *Hum Mol Genet* 20:3841–3851.
- Schagger H, Pfeiffer K. 2000. Supercomplexes in the respiratory chains of yeast and mammalian mitochondria. *EMBO J* 19:1777–1783.
- Trounce IA, Kim YL, Jun AS, Wallace DC. 1996. Assessment of mitochondrial oxidative phosphorylation in patient muscle biopsies, lymphoblasts, and transmittochondrial cell lines. *Methods Enzymol* 264:484–509.
- Tsurusaki Y, Osaka H, Hamanoue H, Shimbo H, Tsuji M, Doi H, Saitsu H, Matsumoto N, Miyake N. 2011. Rapid detection of a mutation causing X-linked leucoencephalopathy by exome sequencing. *J Med Genet* 48:606–609.
- Visapaa I, Fellman V, Vesa J, Dasvarma A, Hutton JL, Kumar V, Payne GS, Makarow M, Van Coster R, Taylor RW, Turnbull DM, Suomalainen A, et al. 2002. GRACILE syndrome, a lethal metabolic disorder with iron overload, is caused by a point mutation in BCS1L. *Am J Hum Genet* 71:863–876.

## SHORT COMMUNICATION

# The diagnostic utility of exome sequencing in Joubert syndrome and related disorders

Yoshinori Tsurusaki<sup>1</sup>, Yasuko Kobayashi<sup>2</sup>, Masataka Hisano<sup>3</sup>, Shuichi Ito<sup>4</sup>, Hiroshi Doi<sup>1</sup>, Mitsuko Nakashima<sup>1</sup>, Hirotomo Saito<sup>1</sup>, Naomichi Matsumoto<sup>1</sup> and Noriko Miyake<sup>1</sup>

Joubert syndrome (JS) and related disorders (JSRD) are autosomal recessive and X-linked disorders characterized by hypoplasia of the cerebellar vermis with a characteristic ‘molar tooth sign’ on brain imaging and accompanying neurological symptoms including episodic hypernoea, abnormal eye movements, ataxia and intellectual disability. JSRD are clinically and genetically heterogeneous, and, to date, a total of 17 causative genes are known. We applied whole-exome sequencing (WES) to five JSRD families and found mutations in all: either *CEP290*, *TMEM67* or *INPP5E* was mutated. Compared with conventional Sanger sequencing, WES appears to be advantageous with regard to speed and cost, supporting its potential utility in molecular diagnosis.

*Journal of Human Genetics* advance online publication, 4 October 2012; doi:10.1038/jhg.2012.117

**Keywords:** *CEP290*; exome sequencing; *INPP5E*; Joubert syndrome; molecular diagnosis; *TMEM67*

Joubert syndrome (JS) and related disorders (JSRD) are autosomal recessive and X-linked disorders characterized by hypoplasia of the cerebellar vermis with the characteristic neuroradiological ‘molar tooth sign’ and accompanying neurological symptoms including dysregulation of breathing pattern, ataxia and developmental delay. JSRD are classified into six subtypes: pure JS, JS with ocular defect, JS with renal defect, JS with oculorenal defects, JS with hepatic defect and JS with orofaciocaudal defects.<sup>1</sup> To date, 17 causative genes have been identified in JSRD: *INPP5E*,<sup>2</sup> *TMEM216*,<sup>3</sup> *AH1*,<sup>4</sup> *NPHP1*,<sup>5</sup> *CEP290*,<sup>6</sup> *TMEM67*,<sup>7</sup> *RPGRIPL*,<sup>8</sup> *ARL13B*,<sup>9</sup> *CC2D2A*,<sup>10</sup> *OFD1*,<sup>11</sup> *TTC21B*,<sup>12</sup> *KIF7*,<sup>13</sup> *TCTN1*,<sup>14</sup> *TMEM237*,<sup>15</sup> *CEP41*,<sup>16</sup> *TMEM138*,<sup>17</sup> and *C5ORF42*.<sup>18</sup> Because of the clinical and genetic heterogeneity in JSRD, it can be very difficult to identify the causative mutations in individual cases.

We encountered five non-consanguineous Japanese families with JSRD (Figure 1a) and molar tooth sign was observed in all patients (Figures 1b–e, Supplementary Table 1). Peripheral blood samples were obtained from patients and their family members after written informed consent was given. To identify causative mutations, we performed whole-exome sequencing (WES) in five probands of the five families (one proband from each family). DNA was processed using the SureSelectXT Human All Exon 50 Mb library or V4 (51 Mb) library (Agilent Technologies, Santa Clara, CA, USA), and sequenced on a Genome Analyzer IIx sequencer (Illumina, San Diego, CA, USA) with 108 bp paired-end reads, or on a HiSeq2000 sequencer (Illumina) with 101 bp paired-end reads and 7 bp index reads.

Image analysis and base calling were performed by Illumina pipeline. Approximately 3.8–6.0 Gb of sequence data were mapped to the human reference genome (GRCh37.1/hg19) with Novoalign or Burrows-Wheeler Aligner. The mean depth of coverage was 55–125 reads, with 88–96% of all coding exons being covered by 5× or more reads.

Out of all variants within exons and ±20-bp intronic regions from the exon–intron boundaries, those registered in dbSNP135, 1000 Genomes and ESP5400 and located within the segmental duplications were removed. Homozygous or compound heterozygous variants of 17 JSRD causative genes were then picked up. In patients 1, 2, 3 and 4 whose DNA was captured by the SureSelectXT Human All Exon 50 Mb library, ~90% of the entire coding regions in 13 of 17 causative genes were covered by 5× reads or more. In patient 5 captured by the V4 (51 Mb) library, >90% of the coding region was covered by 5× reads or more (Supplementary Table 2), indicating that the V4 library offered superior coverage to the SureSelectXT library around the regions of the JSRD genes.

All patients from the five families possessed novel compound heterozygous mutations or a homozygous mutation in known genes later confirmed by Sanger sequencing (Figure 1a): c.1862G>A (p.R621Q)/c.700dupC (p.L234Pfs\*56) in *INPP5E* (9q34.3) for family 1; c.5788A>T (p.K1930\*)/c.6012-12A>T in *CEP290* (12q21.32) for family 2; c.329A>G (p.D110G)/c.2322+5delG in *TMEM67* (8q22.1) for family 3; homozygous c.6012-12A>T in *CEP290* for family 4; and c.214G>T (p.E72\*)/c.6012-12A>T in *CEP290* for family 5. No other variants within 17 known genes have been identified after excluding

<sup>1</sup>Department of Human Genetics, Yokohama City University Graduate School of Medicine, Yokohama, Japan; <sup>2</sup>Department of Pediatrics, Gunma University Graduate School of Medicine, Maebashi, Japan; <sup>3</sup>Department of Nephrology, Chiba Children's Hospital, Chiba, Japan and <sup>4</sup>National Center for Child Health and Development, Tokyo, Japan  
Correspondence: Dr N Miyake, Department of Human Genetics, Yokohama City University Graduate School of Medicine, 3-9 Fukuura, Kanazawa-ku, Yokohama 236-0004, Japan.

E-mail: nmiyake@yokohama-cu.ac.jp

Received 31 July 2012; revised 3 September 2012; accepted 5 September 2012

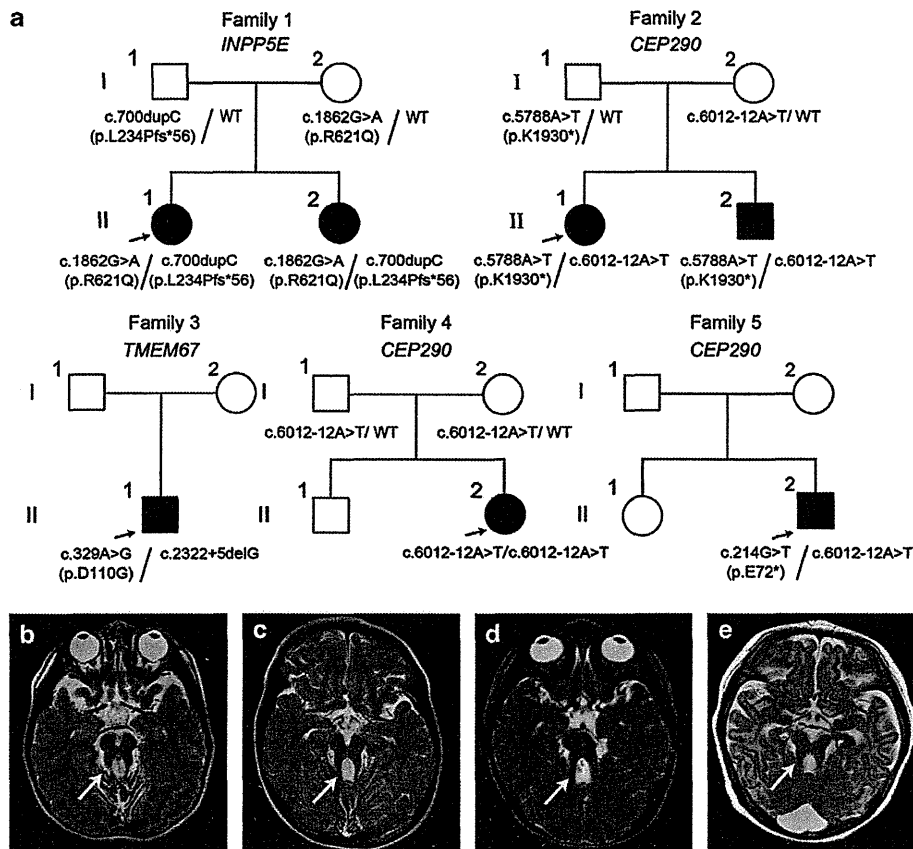


**Figure 1** Familial pedigree and brain MRI of the patients. (a) JSRD families and mutations. (b) T2-weighted axial images of III-1, family 1. (c) T2-weighted axial images of III-2, family 1. (d) T2-weighted axial images of III-1, family 2. (e) T2-weighted axial images of III-2, family 2. The molar tooth sign is visible in all patients (arrowheads).

the variants of dbSNP135, 1000 Genomes and ESP5400. Clinical phenotypes caused by respective mutated genes are discussed in Supplementary text. In families 1, 2 and 4 in which parental samples were available, all parents were heterozygous carriers of one of the mutations. As parental samples were unavailable from families 3 and 5, we determined whether two mutations resided on different alleles by cloning an reverse transcriptase-PCR (RT-PCR) product amplified from total RNA of lymphoblastoid cells into a pCR4-TOPO vector (Life Technologies, Carlsbad, CA, USA) and sequencing. Each mutation was found in a different allele for both families (data not shown). Another variant, c.1894A>G (p.K632E) in *CEP290*, of family 2 was not found to be pathogenic based on web-based analyses such as SIFT, PolyPhen-2 and Mutation Taster (Supplementary Table 3). In families 2, 4 and 5 with a *CEP290* abnormality, c.6012-12A>T was shared. On the basis of our in-house 135 exome data, the allele frequency of the mutation was 1/270 allele (0.74%), indicating that it may be a rare variant in Japanese. The other mutations were not found in our in-house 135 exome data.

Splicing effects were examined in families 3 and 4. RT-PCR was performed on RNA from lymphoblastoid cells of family members using primers spanning exons 42/43 and 45/46 in family 4 and exons 20/21 and 24/25 in family 3 (sequence information available on request). In family 4, only an aberrant cDNA was detected in II-2, whereas the parents (I-1 and I-2) showed two different products including one wild-type, which was detected in a control

(Supplementary Figures 1a, b). Sequencing of the mutant product revealed a 57-bp insertion corresponding to the 3'-side of intron 43. As a result, a premature stop codon was introduced at intron 43. In family 3, RT-PCR detected a mutant cDNA in II-1 together with a wild-type product, which was detected in a control. Sequencing of the mutant product confirmed the skipping of exon 22, resulting in an in-frame 27 amino-acid deletion (Supplementary Figures 1c, d).

WES has proved a powerful tool for the identification of novel genes in genetic diseases. It also has tremendous potential for clinical diagnosis and is now being applied in the molecular diagnosis of single-gene disorders such as neurofibromatosis type 1, Marfan syndrome and multi-gene disorders such as retinitis pigmentosa.<sup>19</sup> As shown here, WES would also be suitable for the diagnosis of JSRD, another multi-gene disorder. Though the read-coverage of the old version of SureSelect did not sufficiently collect genomic DNAs for four genes (*INPP5E*, *TMEM216*, *KIF7* and *TCTN1*), the performance of the V4 (51 Mb) library was satisfactory for all genes. Further, as exome capture technology is based on hybridization it can be refractory to homologous regions, so other methods such as multiplex PCR amplification and multiple microdroplet PCR technology could be useful in addition.

In conclusion, we were able to identify causative mutations in five non-consanguineous families with JSRD using WES. The diagnostic utility of WES is obvious, implying that WES or other next-generation sequencing technologies will be a main factor of molecular diagnosis.

## ACKNOWLEDGEMENTS

We thank the patients and their families for their participation in this study. This work was supported by research grants from the Ministry of Health, Labor and Welfare (HS, N Matsumoto, N Miyake), the Japan Science and Technology Agency (N Matsumoto), the Strategic Research Program for Brain Sciences (N Matsumoto) and a Grant-in-Aid for Scientific Research on Innovative Areas-(Transcription cycle)-from the Ministry of Education, Culture, Sports, Science and Technology of Japan (N Matsumoto), a Grant-in-Aid for Scientific Research from Japan Society for the Promotion of Science (N Matsumoto), a Grant-in-Aid for Young Scientist from Japan Society for the Promotion of Science (HS, N Miyake) and a grant from the Takeda Science Foundation (N Matsumoto, N Miyake).

**Web Resources:** The URLs for data presented herein are as follows: Novoalign, <http://www.novocraft.com/main/index.php>; Burrows-Wheeler Aligner, <http://bio-bwa.sourceforge.net/>; SIFT, <http://sift.jcvi.org/>; PolyPhen-2, <http://genetics.bwh.harvard.edu/pph2/>; Mutation Taster, <http://neurocore.charite.de/MutationTaster/>

- 1 Brancati, F., Dallapiccola, B. & Valente, E. M. Joubert Syndrome and related disorders. *Orphanet. J. Rare Dis.* **5**, 20 (2010).
- 2 Bielas, S. L., Silhavy, J. L., Brancati, F., Kisseleva, M. V., Al-Gazali, L., Sztriha, L. *et al.* Mutations in INPP5E, encoding inositol polyphosphate-5-phosphatase E, link phosphatidylinositol signaling to the ciliopathies. *Nat. Genet.* **41**, 1032–1036 (2009).
- 3 Valente, E. M., Logan, C. V., Mougou-Zerelli, S., Lee, J. H., Silhavy, J. L., Brancati, F. *et al.* Mutations in TMEM216 perturb ciliogenesis and cause Joubert, Meckel and related syndromes. *Nat. Genet.* **42**, 619–625 (2010).
- 4 Ferland, R. J., Eyaid, W., Collura, R. V., Tully, L. D., Hill, R. S., Al-Nouri, D. *et al.* Abnormal cerebellar development and axonal decussation due to mutations in AH11 in Joubert syndrome. *Nat. Genet.* **36**, 1008–1013 (2004).
- 5 Parisi, M. A., Bennett, C. L., Eckert, M. L., Dobyns, W. B., Gleeson, J. G., Shaw, D. W. *et al.* The NPHP1 gene deletion associated with juvenile nephronophthisis is present in a subset of individuals with Joubert syndrome. *Am. J. Hum. Genet.* **75**, 82–91 (2004).
- 6 Valente, E. M., Silhavy, J. L., Brancati, F., Barrano, G., Krishnaswami, S. R., Castori, M. *et al.* Mutations in CEP290, which encodes a centrosomal protein, cause pleiotropic forms of Joubert syndrome. *Nat. Genet.* **38**, 623–625 (2006).
- 7 Baala, L., Romano, S., Khaddour, R., Saunier, S., Smith, U. M., Audollent, S. *et al.* The Meckel-Gruber syndrome gene, MKS3, is mutated in Joubert syndrome. *Am. J. Hum. Genet.* **80**, 186–194 (2007).
- 8 Arts, H. H., Doherty, D., van Beersum, S. E., Parisi, M. A., Letteboer, S. J., Gorden, N. T. *et al.* Mutations in the gene encoding the basal body protein RPGRIP1L, a nephrocystin-4 interactor, cause Joubert syndrome. *Nat. Genet.* **39**, 882–888 (2007).
- 9 Cantagrel, V., Silhavy, J. L., Bielas, S. L., Swistun, D., Marsh, S. E., Bertrand, J. Y. *et al.* Mutations in the cilia gene ARL13B lead to the classical form of Joubert syndrome. *Am. J. Hum. Genet.* **83**, 170–179 (2008).
- 10 Gorden, N. T., Arts, H. H., Parisi, M. A., Coene, K. L., Letteboer, S. J., van Beersum, S. E. *et al.* CC2D2A is mutated in Joubert syndrome and interacts with the ciliopathy-associated basal body protein CEP290. *Am. J. Hum. Genet.* **83**, 559–571 (2008).
- 11 Coene, K. L., Roepman, R., Doherty, D., Afroze, B., Kroes, H. Y., Letteboer, S. J. *et al.* OFD1 is mutated in X-linked Joubert syndrome and interacts with LCA5-encoded lebercilin. *Am. J. Hum. Genet.* **85**, 465–481 (2009).
- 12 Davis, E. E., Zhang, Q., Liu, Q., Diplas, B. H., Davey, L. M., Hartley, J. *et al.* TTC21B contributes both causal and modifying alleles across the ciliopathy spectrum. *Nat. Genet.* **43**, 189–196 (2011).
- 13 Dafinger, C., Liebau, M. C., Elsayed, S. M., Hellenbroich, Y., Boltshauser, E., Korenke, G. C. *et al.* Mutations in KIF7 link Joubert syndrome with Sonic Hedgehog signaling and microtubule dynamics. *J. Clin. Invest.* **121**, 2662–2667 (2011).
- 14 Garcia-Gonzalo, F. R., Corbit, K. C., Sirerol-Piquer, M. S., Ramaswami, G., Otto, E. A., Noriega, T. R. *et al.* A transition zone complex regulates mammalian ciliogenesis and ciliary membrane composition. *Nat. Genet.* **43**, 776–784 (2011).
- 15 Huang, L., Szymanska, K., Jensen, V. L., Janecke, A. R., Innes, A. M., Davis, E. E. *et al.* TMEM237 is mutated in individuals with a Joubert syndrome related disorder and expands the role of the TMEM family at the ciliary transition zone. *Am. J. Hum. Genet.* **89**, 713–730 (2011).
- 16 Lee, J. E., Silhavy, J. L., Zaki, M. S., Schroth, J., Bielas, S. L., Marsh, S. E. *et al.* CEP41 is mutated in Joubert syndrome and is required for tubulin glutamylation at the cilium. *Nat. Genet.* **44**, 193–199 (2012).
- 17 Lee, J. H., Silhavy, J. L., Lee, J. E., Al-Gazali, L., Thomas, S., Davis, E. E. *et al.* Evolutionarily assembled cis-regulatory module at a human ciliopathy locus. *Science* **335**, 966–969 (2012).
- 18 Srour, M., Schwartzentruber, J., Hamdan, F. F., Ospina, L. H., Patry, L., Labuda, D. *et al.* Mutations in C5ORF42 Cause Joubert Syndrome in the French Canadian Population. *Am. J. Hum. Genet.* **90**, 693–700 (2012).
- 19 Zhang, W., Cui, H. & Wong, L. J. Application of next generation sequencing to molecular diagnosis of inherited diseases. *Top. Curr. Chem.* (e-pub ahead of print 11 May 2012; doi:10.1007/128\_2012\_325).

Supplementary Information accompanies the paper on Journal of Human Genetics website (<http://www.nature.com/jhg>)



## Original article

# Neuropathology of leukoencephalopathy with brainstem and spinal cord involvement and high lactate caused by a homozygous mutation of DARS2

Sumimasa Yamashita<sup>a,\*</sup>, Noriko Miyake<sup>b</sup>, Naomichi Matsumoto<sup>b</sup>, Hitoshi Osaka<sup>a</sup>, Mizue Iai<sup>a</sup>, Noriko Aida<sup>c</sup>, Yukichi Tanaka<sup>d</sup>

<sup>a</sup> Division of Child Neurology, Kanagawa Children's Medical Center, Japan

<sup>b</sup> Department of Human Genetics, Yokohama City University Graduate School of Medicine, Japan

<sup>c</sup> Division of Radiology, Kanagawa Children's Medical Center, Japan

<sup>d</sup> Division of Pathology, Kanagawa Children's Medical Center, Japan

Received 23 November 2011; received in revised form 7 April 2012; accepted 9 May 2012

## Abstract

We diagnosed three siblings from consanguineous east Asian parents with leukoencephalopathy with brainstem and spinal cord involvement and high lactate (LBSL) from characteristic MRI, MRS findings and a homozygous mutation in the DARS2 gene. The neurological symptoms of the three patients consisted of psychomotor developmental delay, cerebellar ataxia since infancy, spasticity in the initial phase and peripheral neuropathy in later stages. Their mental development was delayed, but did not deteriorate. MRI signal abnormalities included the same abnormalities reported previously but tended to be more extensive. Signal abnormalities in the cerebral and cerebellar white matter were homogeneous and confluent from early stages. In addition, other tract such as the central tegmental tract was involved. Furthermore, an atrophic change in the cerebral white matter was observed on follow-up in one case. Two of the patients were autopsied and neuropathological findings revealed characteristic vacuolar changes in the white matter of the cerebrum, cerebellum and the nerve tracts of the brain stem and spinal cord. The central myelin sheath showed intralamellar splitting by electron microscopy. These findings were consistent to a spongy degeneration in the diffuse white matter of the brain, or spongiform leukoencephalopathy. In addition, peripheral nerves showed both axonal degeneration and abnormal myelin structures. We discussed the relationship between deficits in mitochondrial aspartyl-tRNA synthetase activity and the neuropathology observed.

© 2012 The Japanese Society of Child Neurology. Published by Elsevier B.V. All rights reserved.

**Keywords:** LBSL; DARS2; MRS; Cerebellar ataxia; Spongy encephalopathy; Axonal degeneration

## 1. Introduction

Recently, the clinical features and magnetic resonance image (MRI) characteristics of leukoencephalopathy with brainstem and spinal cord involvement and lactate

elevation (LBSL) have been described [1]. MRI and <sup>1</sup>H-Magnetic resonance spectroscopy (MRS) of LBSL patients show significant signal abnormalities in the brainstem and spinal cord, as well as cerebral white matter. LBSL is caused by mutations of the DARS2 gene encoding mitochondrial aspartyl-tRNA synthetase (MtAspRS) [2]. DARS2 mutations have been found in all reported patients [2–7], but all have been compound heterozygotes. In this report, we examine a consanguineous family with three individuals affected with LBSL

\* Corresponding author. Address: Division of Child Neurology, Kanagawa Children's Medical Center, Mutsukawa 2-138-4 Minami-ku, Yokohama, Kanagawa 232-8555, Japan. Tel.: +81 45 711 2351; fax: +81 45 721 3324.

E-mail address: syamashita@kcmcc.jp (S. Yamashita).

caused by a homozygous *DARS2* mutation [8], which may explain more severe symptoms than compound heterozygous [9]. Neuropathological examination including autopsies of two of the cases revealed confirmed LBSL. This is the first autopsy report of the patients with LBSL.

## 2. Case report

Three of four siblings were affected by the same disorder. Their parents were consanguineous cousins. In this family, the great-grand father was of Chinese origin and the great-grand mother was Japanese. There were no other family members with the same disorder. The eldest sister, aged 24 years, is healthy, and Case 1 is the second sister affected, but is alive. Cases 2 and 3 were the third and fourth siblings. Both were affected and died of the disorder.

**Case 1:** 23 year old female. Case 1 had no eventful neonatal history. She could walk and speak several words at 1 year old. She suffered from ataxic gait at 3 years, and was admitted to our hospital at 5 years. On examination, hypotonia, horizontal nystagmus, dysdiadochokinesis, intention tremor of upper extremities,

and slurred speech were observed. Deep tendon reflexes (DTRs) in her upper and lower extremities were elicited normally. DTRs disappeared completely at the age of 7 years in her lower extremities and at 13 years in her upper extremities. She lost the ability to walk with support at 7 years, and required a wheel chair. Her mental development was delayed severely. At the current age of 23 years, she is wheel-chair bound, but driving approximately 10 m by herself.

**Case 2:** 8 year old female at autopsy, younger sister of Case 1. Case 2 was able to sit alone at the age of 6 months, but she did not obtain any motor development. She showed ataxia, mild muscle hypertonia, hyperreflexia in Achilles tendon reflex, positive Babinski reflex, positive foot clonus, intention tremor, nystagmus, slurred speech, and mental retardation at 5 years old. Her muscle tonus turned to hypotonus at 8 years. She died from respiratory distress and pneumonia at 8 years.

**Case 3:** 2 year old male at autopsy, younger brother of Case 1. Case 3 could sit alone at the age of 5 months and walk with support at the age of 1 year and 4 months. He could speak several words at that time, although he showed ataxia. At age 2, his muscle tonus was increased

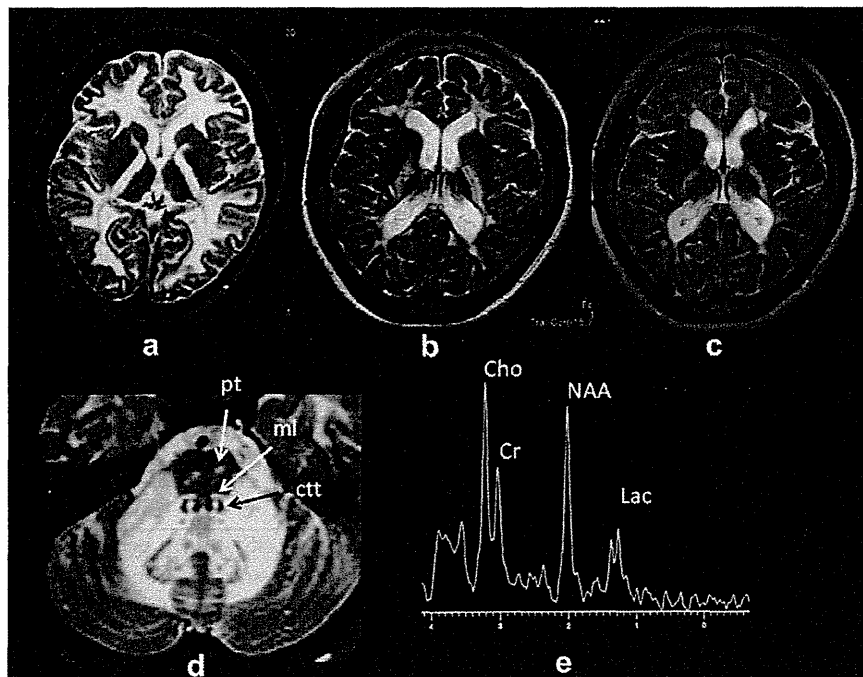


Fig. 1. MRI and MR spectroscopy of Case 1. (a) T2-WI of the cerebrum at 10 years old. (b) T2-WI of the cerebrum at 18 years old. (c) T2-WI of the cerebrum at 22 years old. (d) T2-WI. Pons and cerebellum at 10 years old. pt, pyramidal tract; ml, medial lemniscus; ctt, central tegmental tract. (e) MR spectroscopy of the cerebral white matter at 10 years old. Cho, choline; Cr, creatine; NAA, N-acetyl aspartic acid; Lac, lactate (PRESS sequence, TR/TE = 2000/270). There was homogeneous diffuse prolongation of T1 and T2 signals in the entire cerebral white matter that extended from immediately below the cortex to the deep white matter in all three cases [8]. As a result, U-fibers were spared well in the frontal lobe, moderately in parietal and temporal lobe, but were not preserved in the occipital lobe. The same strong signal abnormalities as the cerebral white matter were seen in the posterior limb of the internal capsule in all cases. Progressive atrophic change in cerebral white matter including the posterior limb of the internal capsule developed gradually, which MRI demonstrated at the age of 10, 18 and 22 years (a–c). Marked involvement of the diffuse white matter of the cerebellum and of the central tegmental tracts was observed (d). MR spectroscopy showed high lactate level at the age of 10 years (e).

and he had hyperreflexia, positive Babinski reflex, and horizontal nystagmus, but no tremor in his fingers. He expired from respiratory failure after febrile illness at age 2.

A detailed biochemical examination was performed in all three patients, but revealed no definite abnormalities. Serum lactate levels in each patient were within normal limits, although cerebrospinal fluid (CSF) lactate was no more than a borderline elevation. In Case 1, CSF lactate was 24.3 mg/dl (normal range <ca.23). In each case, motor nerve conduction velocity (MCV) was within the normal range in infancy, but decreased gradually, and the amplitudes of compound muscle action potential was decreased since the infantile ages. In Case 1, MCV showed 50 m/sec at the median nerve at the age of 10. EMG showed a neurogenic pattern in the upper extremity and fibrillation in the lower extremity. In Case 3, MCV showed 42.3 m/sec in the median nerve at the age of 2 years.

The MRI findings of the three cases (Fig. 1) revealed similar features and meet the criteria of LBSL described by the previous report [1]. The findings of our cases, however, were characterized by the following four points. First, similar strenuous and diffuse cerebral white matter involvement was observed in all three cases. Second, progressive atrophic change in cerebral white matter developed gradually, which MRI demonstrated at the age of 10, 18 and 22 years in Case 1 (Fig. 1a–c). Third, marked diffuse involvement of the white matter of the cerebellum

was observed (Fig. 1d). Fourth, marked involvement of the central tegmental tracts was observed (Fig. 1d).

By MR spectroscopy, high lactate levels were observed in Cases 1 (Fig. 1e) and 3. Reexamination of Case 1 at age 22 years revealed a slight elevation of lactate, but it was lower than that at 10 years.

Direct sequencing of *DARS2* gene revealed a homozygous c.228-22T>A in the three affected and heterozygous c.228-22T>A in the parents and healthy sister. This intronic mutation change led to the skipping of exon 3, low transcription, and faint protein level in proband fibroblasts [8]. Therefore, a diagnosis of LBSL was obtained in our cases.

### 3. Neuropathology

We re-evaluated the autopsy finding of Cases 2 and 3 retrospectively and clarified the disease mechanism after obtaining the result of genetic analysis. In both patients, neuropathological findings were similar in the central nervous system. Vacuolar changes in the cerebral white matter began immediately below the cortex (Fig. 2a). Deeper, the more spongy alterations were observed as a large number of vacuoles and astrocytes in the white matter (Fig. 2b). The neuropil was rarefacted, and many macrophages had infiltrated into the deep white matter. As a result, demyelination and axonal degeneration was observed in the deeper white matter. The central myelin sheath showed intralamellar splitting of the outermost

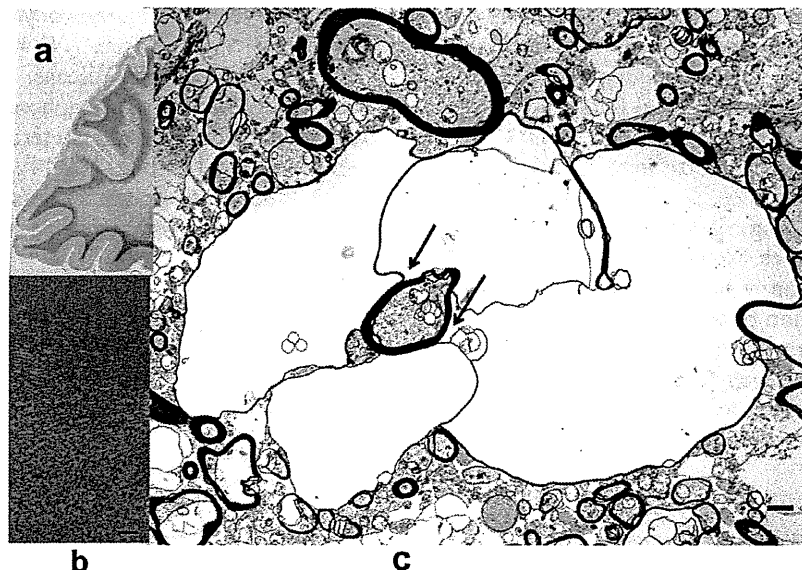


Fig. 2. Neuropathological findings of the cerebrum. (a) Frontal lobe of the cerebrum of Case 2. KB stain. Myelin pallor is diffuse in the cerebral white matter. (b) Microscopic finding of frontal lobe of the cerebrum of Case 2. KB stain. Vacuolar changes in the cerebral white matter began immediately below the cortex (top). The subcortical U-fibers were spared in the frontal lobe and myelinated fibers were preserved. The deeper (bottom) regions show more spongy alterations. A large number of vacuoles and astrocytes exist in the white matter. Scale 100  $\mu$ m. (c) Electron microscopic findings of the cerebrum of Case 3. The central myelin sheath shows intralamellar splitting ( $\leftarrow$ ) of the outermost myelin lamellae. Scale 1  $\mu$ m.

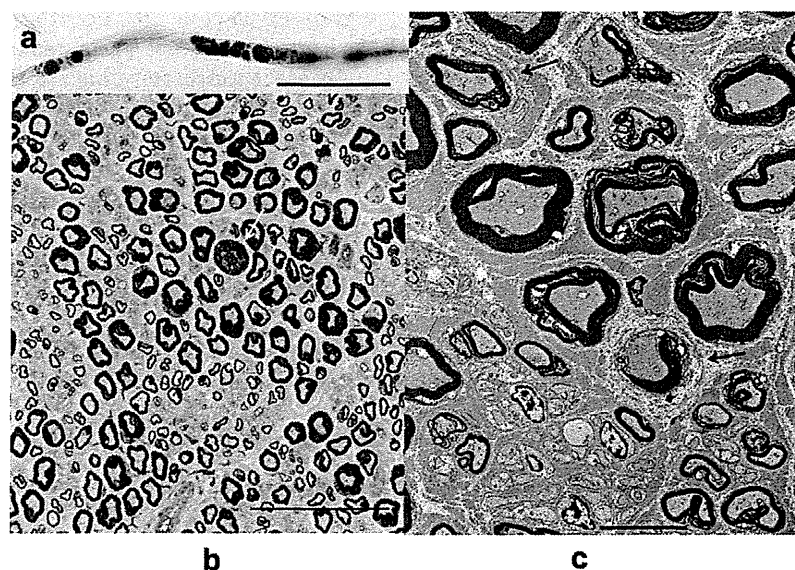


Fig. 3. Neuropathological findings of the autopsied sural nerve of Case 3. (a) Microscopy of the sural nerve by teased fiber examination. Typical formation of many myelin ovoids along a myelinated fiber is observed. Scale 100  $\mu\text{m}$ . (b) Epon-embedded semi-thin section with toluidine blue staining. The numbers of myelinated nerve fibers is reduced mildly or moderately with an extracellular endoneurial connective tissue expansion. Abnormal myelin layer folding, myelin separation at the inside of layers, partial myelin clusters of various sizes associated with myelin separation and partial thin myelin layers were characteristic. Axonal degeneration ( $\leftarrow$ ) within several myelinated fibers is observed. Scale 50  $\mu\text{m}$ . (c) Electron microscopic findings of the sural nerve. Abnormal myelin layer folding, myelin separation at the inside of layers, partial myelin clusters of various sizes and partial thin myelin layers are observed. Onion bulb formation ( $\leftarrow$ ) is seen surrounding a few myelinated fibers by poor Schwann cell cytoplasm, but atypical onion bulb was recognized frequently in several layers of basal lamina, and abnormal Schwann cell processes around unmyelinated fibers were observed. No abnormal crystalline structure was observed in the mitochondria. Scale 10  $\mu\text{m}$ .

myelin lamellae by electron microscopic examination (Fig. 2c). The cerebral cortical layers showed normal structures and no abnormal storage materials in the neuronal cells. Purkinje cells of the cerebellum were lost moderately and Bergmann's glial cells were increased. Cerebellar white matter showed similar alteration as the cerebrum. The neuropathological findings indicated spongy degeneration of the white matter.

The sural nerve was investigated in three cases. In the teased fiber examination (Fig. 3a), typical formation of many myelin ovoids along a few myelinated fibers was observed in all three cases. Neither segmental demyelination nor remyelination was a predominant feature. Microscopic examination revealed that the numbers of myelinated nerve fibers was reduced mildly or moderately (Fig. 3b). Axonal degeneration within several myelinated fibers was observed in Cases 1 and 3.

#### 4. Discussion

The pathologically characteristic findings revealed a spongy degeneration in the diffuse white matter of the brain. This pathological finding is apparent in many inherited metabolic and degenerative neurological disorders [10–12]. Intralamellar split of the myelin sheaths contributed to forming variable vacuoles in the white matter. In addition, a noteworthy finding was axonal

degeneration of the peripheral nerves in our patients. This finding is an important feature of LBSL as described by Isohanni et al. [4]. Mutations in the genes encoding cytoplasmic aminoacyl-tRNA synthetases for glycine [13] and tyrosine [14] have been identified in Charcot–Marie–Tooth disease. Both disorders show axonal degeneration of peripheral nerves because these synthetases localize to axonal termini and have a specific role in neuronal endings [13–14]. In our cases, aspartyl-tRNA synthetase deficiency has proved to induce an axonal type peripheral neuropathy.

#### Conflicts of interest

The authors have no conflict of interest to declare.

#### References

- [1] Van der Knaap MS, van der Voorn P, Barkhof F, van Costr R, Klägeloh-Mann I, Feigenbaum A, et al. A new leukodystrophy with brainstem and spinal cord involvement and high lactate. *Ann Neurol* 2003;53:252–8.
- [2] Scheper GC, van der Klok T, van Andel R, van Berkel CGM, Sissler M, Smet J, et al. Mitochondrial aspartyl-tRNA synthetase deficiency causes leukoencephalopathy with brain stem and spinal cord involvement and lactate elevation. *Nat Genet* 2007;39:534–9.
- [3] Uluc K, Baskan O, Yildirim KA, Ozsahin S, Koseoglu M, Isak B, et al. Leukoencephalopathy with brain stem and spinal cord involvement and high lactate: a genetically proven case with distinct MRI findings. *J Neurol Sci* 2008;273:118–22.



- [4] Isohanni P, Linnankivi T, Buzkova J, Lönnqvist T, Pihko H, Valanne L, et al. DARS2 mutations in mitochondrial leukoencephalopathy and multiple sclerosis. *J Med Genet* 2010;47:66–70.
- [5] Lin J, Chiconelli Faria E, Da Roccha AJ, Rodrigues Masruha M, Pereira Vilanova LC, Scheper GC, et al. Leukoencephalopathy with brainstem and spinal cord involvement and normal lactate: a new mutation in the DARS2 gene. *J Child Neurol* 2010;25:1425–8.
- [6] Mierzevska H, van der Knaap MS, Scheper GC, Bekiesinska-Figatowska M, Szczepanik E, Jurkiewicz E. Leukoencephalopathy with brain stem and spinal cord involvement and high lactate elevation in the first Polish patient. *Brain Dev* 2011;33:713–7.
- [7] Labauge P, Dorboz I, Eymard-Pierre E, Dereeper O, Boespflug-Tanguy O. Clinically asymptomatic adult patient with extensive LBSL MRI pattern and DARS2 mutations. *J Neurol* 2011;258:335–7.
- [8] Miyake N, Yamashita S, Kurosawa K, Miyatake S, Tsurusaki Y, Doi H. A novel homozygous mutation of DARS2 may cause a severe LBSL variant. *Clin Genet* 2011;80:293–6.
- [9] Bonnefond L, Fender A, Rudinger-Thirion J, Giege R, Florentz C, Sissler M. Toward the full set of human mitochondrial aminoacyl-tRNA synthetases: characterization of AspRS and TyrRS. *Biochemistry* 2005;44:4805–16.
- [10] Van der Knaap MS, Barth PG, Gabreëls FJM, Franzoni E, Begeer JH, Stroink H, et al. A new leukoencephalopathy with vanishing white matter. *Neurology* 1997;48:845–55.
- [11] Van der Knaap MS, Barth PG, Vrensen GFJM, Valk J. Histopathology of an infantile-onset spongiform leukoencephalopathy with a discrepantly mild clinical course. *Acta Neuropathol* 1996;92:206–12.
- [12] Yamashita S, Iwamoto H, Hara M, Arai N. Infantile spongiform leukoencephalopathy: clinical and pathologic findings. *Pediatr Neurol* 2002;27:217–20.
- [13] Antonellis A, Ellswoorth RE, Sambuugin N, Puls I, Abel A, Lee-Lin SQ, et al. Glycyl tRNA synthetase mutations in Charcot-Marie-Tooth disease type 2D and distal spinal muscular atrophy type V. *Am J Hum Genet* 2003;72:1293–9.
- [14] Jordanova A, Irobi J, Thomas FP, Van Dijk P, Meerschaert K, Dewil M, et al. Disrupted function and axonal distribution of mutant tyrosyl-tRNA synthetase in dominant intermediate Charcot-Marie-Tooth neuropathy. *Nat Genet* 2006;36:197–202.

## Hypothalamic pituitary complications in Kabuki syndrome

Naoko Ito · Kenji Ihara · Yasushi Tsutsumi ·  
Noriko Miyake · Naomichi Matsumoto ·  
Toshiro Hara

© Springer Science+Business Media, LLC 2012

**Abstract** Kabuki syndrome is characterized by distinctive facial features, multiple anomalies and mental retardation. In this syndrome, structural CNS abnormalities are commonly observed, but congenital abnormalities in the pituitary gland or hypothalamus have rarely been reported. We searched the published medical literature on the complications in hypothalamic pituitary axis in this syndrome. As a result, only nine patients with Kabuki syndrome had been reported to have complications in hypothalamic pituitary axis in previous papers. Among the nine reported patients and one presented case in this report, GH deficiency was the most frequent complication and found in six patients. Precocious puberty and central diabetes insipidus (DI) was identified in two cases, respectively, and ACTH deficiency was found in one. One case had combination of GH deficiency and central DI. Three of the 10 patients demonstrated abnormal pituitary findings in MRI study. Two of the six patients with GH deficiency were accompanied with premature thelarche. This review highlights that patients with Kabuki syndrome could present various clinical manifestations due to abnormalities in hypothalamic pituitary axis.

**Keywords** Kabuki syndrome · Central diabetes insipidus · Hypothalamic pituitary axis · *MLL2* gene

---

N. Ito · K. Ihara (✉) · Y. Tsutsumi · T. Hara  
Department of Pediatrics, Graduate School of Medical Sciences,  
Kyushu University, 3-1-1, Maidashi, Higashi-ku,  
Fukuoka 812-8582, Japan  
e-mail: k-ihara@pediatr.med.kyushu-u.ac.jp

N. Miyake · N. Matsumoto  
Department of Human Genetics, Graduate School of Medicine,  
Yokohama City University, Yokohama, Japan

### Abbreviations

AVP	Arginine-vasopressin
CNS	Central nervous system
DDAVP	1-deamino-8-D-arginine vasopressin
DI	Diabetes insipidus
eGFR	Estimated glomerular filtration rate
GH	Growth hormone
MLL	Mixed lineage leukemia
MRI	Magnetic resonance imaging

### Introduction

Kabuki syndrome is a rare, multiple malformation disorder characterized by a distinctive facial appearance, cardiac anomalies, skeletal abnormalities, immunological defects and mental retardation [1, 2]. Besides these typical manifestations, clinical symptoms and congenital abnormalities are considerably variable. Malformation in central nervous system are frequently observed in this syndrome with great differences [3], whereas, congenital abnormalities in the pituitary gland or hypothalamus have rarely been reported. In particular, central diabetes insipidus (DI) in a patient with Kabuki syndrome has only been reported in one previous paper [4]. We herein briefly report a case of Kabuki syndrome with central DI who presented with polydipsia and polyuria. Then, we searched the published medical literature on the complications in hypothalamic pituitary axis in Kabuki syndrome.

### Case report

The patient was born at term from non-consanguineous parents with no family history of congenital malformations.

**Table 1** Clinical features for Kabuki syndrome in the patient at 8 years of age

Craniofacial abnormality	
Characteristic face	+
Microcephaly	-
Long palpebral fissures	+
Epicanthus	+
Lower palpebral eversion	+
Ptosis	+
Strabismus	-
Blue sclera	-
Short nasal septum	-
Prominent forehead	-
Arched eyebrows	+
Prominent ear	+
Depressed nasal tip	+
Auticualr deformity	-
Preauricular pits/tags	-
Abnormal dentition	-
Hypodontia	+
High-arched palate	+
Micrognathia	+
Cleft lip/cleft palate	+
Lower lip pits	+
Lower posterior hairline	+
Bone abnormality	
Skeletal abnormality	-
Short 5th finger	+
Clinodactyly (V)	+
Spine/rib abnormality	+
Scoliosis	-
Hip joint dislocation	-
Dermatoglyphic findings	
Abnormal dermatoglyphic findings	+
Prominent finger tip pads	+
Neurological abnormality	
Developmental delay	+
Intellectual disability	+
Hypotonia	-
Hypotonia in infancy	+
Seizure	+ <sup>a</sup>
Brain atrophy	-
CNS malformation	-
Stature	
Short stature	+ <sup>b</sup>
Prenatal growth retardation	-
Postnatal growth retardation	+
Visceral abnormality	
Generalized hirsutism	-
Cardiovascular abnormality	+
Umbilical hernia	-

**Table 1** continued

Kidney/uterther malformation	+ <sup>c</sup>
Kidney dysfunction	+ <sup>d</sup>
Cryptorchism	-
Anogenital anomaly	-
Liver abnormality	-
Spleen abnormality	-
Hormonal abnormality	+ <sup>e</sup>
Others	
Joint laxity	+
Recurrent otitis media	+
Deafness	-
Premature thelarche	+
Neonatal hyperbilirubinemia	+
Obesity	-
Anemia	-

<sup>a</sup> Afebrile seizures<sup>b</sup> -4.03 SD at 8 years of age<sup>c</sup> Hypoplastic and malpositioned right kidney<sup>d</sup> eGFR = 48–122 ml/min/1.73 m<sup>2</sup> at 8 years of age<sup>e</sup> Central diabetes insipidus

She was doing well at birth, and her birth weight was 2,915 g. A physical examination detected a cleft in the soft palate, which caused feeding difficulties requiring tube feeding until the cleft closure operation was performed at 2 years of age. She also had a ventricular septal defect, which closed spontaneously by 1 year of age. At the age of 1 year, she was diagnosed to have Kabuki syndrome on the basis of her characteristic facial appearance, including long palpebral fissures, lower palpebral eversion, arched eyebrows, lower lip pits, a depressed nasal tip and prominent ears, with distinctive symptoms of short 5th fingers and prominent finger tip pads (Table 1). At 5 years of age, a routine examination by abdominal ultrasound imaging detected a hypoplastic and malpositioned right kidney. This renal malformation was asymptomatic, but careful check-ups for her renal function were started then. At 6 years of age, polydipsia and polyuria gradually emerged, and the patient was referred to our hospital at the age of 8 years for evaluation of her renal function, because her serum creatinine levels were transiently elevated to 0.52–0.91 mg/dL (eGFR = 48–84 ml/min/1.73 m<sup>2</sup>) during the time.

At the admission, the patient's height and weight were 105.7 cm (-4.03 standard deviation) and 16.6 kg. Her serum BUN and creatinine levels were 14 and 0.36 mg/dL, respectively (eGFR = 122 ml/min/1.73 m<sup>2</sup>), therefore, her polydipsia and polyuria might not be explained by secondary nephrogenic diabetes insipidus due to the hypoplastic kidney, and the transient increase of serum creatinine levels had been probably derived from mild

**Fig. 1** The results of the water deprivation test and the subsequent administration of AVP. The time course of the serum ADH levels or serum and urine osmotic pressures after starting water deprivation are shown. AVP administration at 4 h after water deprivation decreased the urine output and increased the urine osmotic pressure appropriately. N/A, not assessed

	Water deprivation starting				AVP administration		
	0 hr	1 hr	2 hr	3 hr	4 hr	1 hr	2 hr
ADH (pg/ml)	1.4	1.5	1.7	1.4	1.5	N/A	N/A
Serum osmotic pressure (mOsm)	287	286	287	290	291	N/A	N/A
Urine osmotic pressure (mOsm)	86	115	270	395	451	550	560
Urine volume /hr (mL/hr)	N/A	60	30	20	20	N/A	N/A

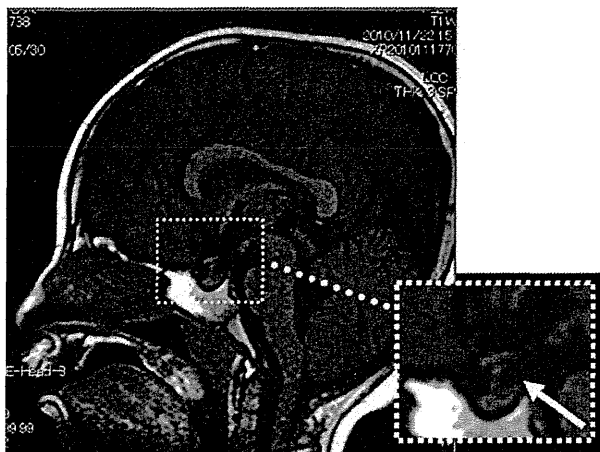


**Fig. 2** The sagittal section of T1-weighted brain MRI. A rectangle area bounded by dotted lines is enlarged to show the details of the pituitary gland and its surrounding region. The arrow indicates the absence of a high intensity signal of the posterior lobe in pituitary gland

dehydration by polyuria. The following data about the serum arginine-vasopressin (AVP) level and serum/urine osmolarity ratio indicated the existence of impaired AVP secretion. A water deprivation test and the subsequent administration of AVP showed that endogenous vasopressin was not appropriately secreted (Fig. 1). T1-weighted magnetic resonance imaging (MRI) of the brain demonstrated the absence of a high intensity signal of the posterior lobe in the pituitary gland, without cell infiltration or inflammation in the hypothalamus or pituitary gland (Fig. 2). There were no other anatomical abnormalities in the brain. The laboratory data that would suggest the co-existence of autoimmune disease, such as anti-nuclear antibodies, rheumatoid factor or anti-pituitary gland antibodies, were all negative, and the serum immunoglobulin and complementary factor levels were within the normal range.

After starting the administration of 1-deamino-8-D-arginine vasopressin (DDAVP), the polydipsia and polyuria drastically disappeared. The basal levels of the anterior pituitary hormones and related factors were within normal ranges as follows: plasma ACTH, 12.9 pg/ml; serum cortisol, 16.4 µg/dl; LH, <0.2 U/L; FSH, 3.5 U/L; prolactin, 5.2 ng/ml; TSH, 3.80 microU/mL; free T4, 1.74 ng/dL. A growth hormone (GH) provocative test by intravenous arginine administration showed normal GH secretion (peak value 8.5 ng/ml at 60 min). The IGF-1 level was low (42 ng/ml; normal range, 95–437), but was recovered to the normal level (118 ng/ml) 5 months after starting AVP treatment. She was then annually performed the MRI follow-up evaluation. The sequence analysis of the *MLL2* gene did not detect any mutations in the coding regions. Besides the previously reported SNPs, a novel non-synonymous SNP; c.8813C > T, p.Pro2938Leu, was identified in the *MLL2* gene of the patient, and was transmitted from her asymptomatic father. This SNP was found in 4 in 363 normal individuals (allele frequency, 0.55 %).

#### Review of complications in hypothalamic pituitary axis in Kabuki syndrome

To the best of our knowledge, only nine patients with Kabuki syndrome had been reported to have complications in hypothalamic pituitary axis in previous papers [4–12]. Among the 10 patients including the present case, GH deficiency was the most frequent complication and found in six patients [4, 5, 8, 9, 11, 12]. Next, precocious puberty and central DI was identified in two cases [4], respectively, and ACTH deficiency was found in one [6]. One case had combination of GH deficiency and central DI [4]. Three of the 10 patients demonstrated abnormal pituitary findings in MRI study [4, 12]. Two of the six patients with GH deficiency were accompanied with premature thelarche [8, 11].